Nanoscale

High-Rate Potassium Ion and Sodium Ion Batteries by Co-Intercalation Anodes and Open Framework Cathodes

Journal:	*Nanoscale*
Manuscript ID	NR-COM-02-2018-001685.R1
Article Type:	Communication
Date Submitted by the Author:	19-Jun-2018

Complete List of Authors:	Moyer, Kathleen; Vanderbilt University, Materials Science Donohue, Jennifer; Vanderbilt University, Mechanical Engineering Ramanna, Neha; Vanderbilt University, Mechanical Engineering Cohn, Adam; Vanderbilt University, Mechanical Engineering Muralidharan, Nitin; Vanderbilt University, Materials Science Eaves, Janna; Vanderbilt University, Mechanical Engineering Pint, Cary; Vanderbilt University, Mechanical Engineering

High-Rate Potassium Ion and Sodium Ion Batteries by Co-Intercalation Anodes and Open Framework Cathodes

Kathleen Moyer[a], *Jennifer Donohue*[a], *Neha Ramanna*[a], *Adam P. Cohn*[b], *Nitin Muralidharan*[a], *Janna Eaves*[b], *Cary L. Pint*[a, b] *

[a]Interdisciplinary Materials Science Program, Vanderbilt University, Nashville, TN 37235

[b]Department of Mechanical Engineering, Vanderbilt University, Nashville, TN 37235

KEYWORDS: co-intercalation, graphite, Prussian blue, open framework cathodes, potassium-ion batteries, sodium-ion batteries, fast-charging

*Corresponding Author: cary.l.pint@vanderbilt.edu

Abstract

Here we demonstrate a full-cell battery design that bridges the energy density and rate capability between that of supercapacitors or pseudocapacitors with that of traditional lithium-ion batteries. This is accomplished by pairing an anode that enables ultrafast ion co-intercalation, an open framework cathode that allows rapid ion diffusion, and linear ether based electrolyte that sustains cell-level stability and high rate performance. We show this platform to be suitable for both sodium and potassium batteries using graphite as the co-intercalation anode, and Prussian blue as the open framework cathode. Our devices exhibit active material energy densities > 100 Wh/kg with power density > 1000 W/kg with cycling durability approaching ~ 80% energy density retention over 2000 cycles. This work brings together state-of-the-art concepts for fast-charging batteries into a full-cell configuration.

Introduction

Whereas many applications, such as consumer electronics, can suffice with the energy and power density of conventional lithium-ion batteries, many future applications that will pivot on battery technology will demand faster charging times. This is especially true for numerous areas such as high power weaponry, EVs or drones conducting long distance travel, and robotics or other high power machinery.[1-3] To this regard, fast recharging and high power density is the focus of high power electrochemical supercapacitors, although even the most novel approaches in such systems remain limited to energy density many times lower than a battery due to electrolyte, cell packaging, and the nature in which charge is stored.[4-10] The energy stored per active site for a supercapacitor is much less compared to the energy stored per active site for a faradaic system. Similarly, pseudocapacitors and hybrid capacitors are largely centered on the use of aqueous electrolytes that may enable high power, but at the cost of energy density and commercially viable materials in a packaged device.[11-19] Therefore, there remains a significant need to design devices that can boast the energy density competitive with a battery, but with fast charging capability and durability.

One of the key challenges in fast charging batteries is the diffusion kinetics of ions across the liquid-solid interface, and through the host insertion materials where they are stored. In the first case, this is associated with the de-solvation step of ion insertion into the host material, and in some cases, the diffusion of the ion through the solid-electrolyte interphase (SEI) region.[20] In anode materials such as graphite, the de-solvation of an alkali ion is the rate-limiting step for high power capability.[21] To address this, recent work has highlighted the mechanism of co-intercalation for both sodium (Na) and potassium (K) ions that leverages a solvent which chelates with the alkali metal ion where the solvent forms a shell around the ion.[22-30] This

enables the insertion of the ion and solvent shell into a layered anode, such as graphite or multi-layered graphene, where the rate-limiting de-solvation process is mitigated and the weak ion-host lattice interactions facilitate ultrafast diffusion.[31, 32] Recent work has demonstrated extraordinary results for half-cell devices that utilize co-intercalation, with sodium boasting capacities exceeding 100 mAh/g for over 8000 cycles in nanostructured carbons, and charge times as low as 12 seconds,[33] and potassium demonstrating capacities up to 100 mAh/g with rate capability up to 30 second charge.[34] Whereas researchers have emphasized this mechanism to be transferrable across different ions and different high quality graphite-like materials, the bottleneck of co-intercalation studies to date remains the challenge of combining these half-cell studies into full-cell configuration that can exploit this high rate performance.

In this regard, separate research efforts have been focused on improving the performance of cathode materials. Prussian blue (PB) has been lauded as a promising battery cathode for high rate capability alternative ion chemistries due to its high theoretical capacity (170 mAh/g),[35] rigid, open structure with large interstitial sites,[36, 37] and nontoxic nature and low cost,[38] which is advantageous for large scale applications. This metal organic framework[39] has a hexacyanometalate structure[40] with chemical formula $A_xM[M(CN)_6]_{1-y}{\cdot}zH20$,[41] where A represents alkali ions (Na, K), $0<x<2$, and M represents transition metals. As observed by previous work, the use of iron as the transition metal to synthesize sodium/potassium hexacyanoferrate yields higher capacity and cycling stability compared with other PB analogues.[42] The rigid, open framework cathode structure[43, 44] has large interstitial sites which aid in accommodating corresponding changes in volume during cycling with low lattice strain,[45] and tunable, three-dimensional channels that allow for ion, and even molecule, insertion/extraction.[36, 46] As a result of the electrochemical practicality, there is a strong

correlation between the structure of Prussian blue and performance making it an ideal cathode for high rate battery systems.[47-51]

In this work, we build from previous studies with an aim toward a synergistic cathode – electrolyte- anode battery configuration that leverages the open framework cathode structure and co-intercalation anodic mechanism into a high rate battery device. Our work demonstrates a broadly adaptable design strategy to tailor the performance of a battery to perform with energy density and cycling performance characteristic of a battery, but at high rates often limited to supercapacitors or pseudocapacitors. This enables a class of energy storage systems optimized for higher power applications, such as grid-storage, weaponry, power beaming, electric vehicles, among other next-generation application areas.

Experimental Details

Prussian Blue Synthesis

Sodium Hexacyanoferrate – Sodium Prussian Blue (NaPB): 3 mmol $FeCl_2 \cdot 4H_2O$ (Sigma-Aldrich, >99%) and 2.0 g $Na_3C_6H_5O_7 \cdot 2H_2O$ (Fisher Scientific) were added to 100 mL deionized water to make solution A and stirred until dissolved. 2 mmol $Na_4Fe(CN)_6 \cdot 10H_2O$ (Sigma-Aldrich, >99%) and excess of NaCl (Fisher Scientific, 99.8%) were added to 100 mL deionized water to make solution B and stirred until dissolved. Potassium Hexacyannoferrate – Potassium Prussian Blue (KPB): 3 mmol $FeCl_2 \cdot 4H_2O$ (Sigma-Aldrich, >99%) and 2.0 g $C_6H_5K_3O_7 \cdot H_2O$ (Sigma-Aldrich, >98%) were added to 100 mL deionized water to make solution A and stirred until dissolved. 2 mmol $K_4Fe(CN)_6 \cdot 3H_2O$ (Sigma-Aldrich, 98.5-102.0%) and excess of KCl (Sigma-Aldrich, 99.0-100.5%) were added to 100 mL deionized water to make solution B and stirred until dissolved. In both cases solution B was added to solution A and stirred for 4 hours.

The composite solution was collected by centrifugation and the precipitate was dried at 100˚C overnight. Particle size, morphology, and composition was examined using SEM and EDS with a Zeiss Merlin scanning electron microscope. Material crystal structure was examined by x-ray diffraction using a Rigaku Smart Lab with a Cu Kα radiation source.

Electrode Fabrication

Graphite electrodes were fabricated by making a slurry of natural graphite powder (Alfa Aesar, 99.9995%), conductive carbon black (MTI), and PVDF binder (MTI, >99.5%) in the ratio of (80:10:10) and coated onto carbon coated aluminum (MTI, >99.9%). Similarly, Prussian blue electrodes were fabricated by making a slurry of the synthesized Prussian blue powder (either K- or Na- hexacyanoferrate), multi wall carbon nanotubes (CheapTubes, >95%), and sodium carboxymethyl cellulose (Sigma-Aldrich) in the ratio of (80:10:10) and coated onto carbon coated aluminum (MTI, >99.9%).

Coin Cell Assembly & Electrochemical Testing

Graphite half-cells were fabricated using the graphite electrodes as the working electrode with either Na (Strem Chemicals, 99.95%) or K (Sigma-Aldrich, 99.95%) metal as the counter and reference electrode. Prussian blue half-cells were made using the Prussian blue electrodes as the working electrode with either Na or K metal as the counter and reference electrode. Full-cells were assembled using the graphite electrodes as the anode and Prussian blue electrode as the cathode with a cathode to anode ratio of 1.6:1 by mass with cathode loading of ~0.8 mg/cm^2 and anode loading of ~0.5 mg/cm^2. A 2325 Celgard separator and whatman glass fiber separator were used to fabricate all coin cells. The electrolytes used for all coin cells were 1 M $NaPF_6$ (Alfa Aesar, >99%) in diglyme (Sigma-Aldrich, 99.5%) for Na chemistries and 1 M KPF_6 (Sigma-Aldrich, 99.5%) in diglyme (Sigma-Aldrich, 99.5%) for K chemistries. Cells were

fabricated with extra care to dry the electrolyte using 4Å molecular sieves before use. Electrochemical testing was performed on a multichannel Metrohm Autolab testing apparatus and MTI 8 Channel Battery tester.

Results and discussion

To develop a fast charging battery that relies upon co-intercalation at the anode, and an open framework cathode architecture, we first characterized each type of electrode material in a half-cell configuration (Fig. 1). Both Na^+ and K^+ charge storage in natural graphite *via* co-intercalation was explored using diglyme (DEGDME) solvent using half-cells: Na|$NaPF_6$ in DEGDME|GR and K|KPF_6 in DEGDME|GR. As the coordinated alkali ions and solvent molecule co-intercalate into the graphite, the spacing between the graphene sheets in the c-direction increases and reversibly restores its original structure upon extraction[28] (Fig. 1a). Galvanostatic cycling can be observed in Fig. 1b as the half-cells are charged and discharged and the alkali ions are inserted and extracted into the graphite, respectively. The rate capability of natural graphite as a co-intercalation anode was galvanostatically tested and the results can be found in Fig. S8. Similarly, half-cells of alkali metal Na or K and the respective PB electrode, Na|$NaPF_6$ in DEGDME|NaPB (NaPB) and K|KPF_6 in DEGDME|KPB (KPB), were made to study the synthesized Prussian blue in the diglyme system. Fig. 1c and galvanostatic charge-discharge curves for both the NaPB and KPB electrode materials illustrate the alkali ions moving out of the PB structure on charge and back into the PB open framework on discharge for both Na and K chemistries (Fig. 1c, d). The rigid structure and large interstitial sites[38] of this perovskite-type structure[35] metal organic framework facilitate the intercalation process, allowing for high rate capability, as further demonstrated in this study. Further, scanning electron microscopy (SEM) of the as-synthesized PB particles are shown in Figs. 2c and 2d. KPB particles are more

spherical in morphology (Fig. 2d) compared with the NaPB (Fig. 2c) which are more cubic, corresponding to past literature observations.[35, 38, 42, 43] Both NaPB and KPB particles are ~100 nm in diameter with the particle size of NaPB is ~100nm in diameter while that of KPB is < 100nm, yielding capacities consistent with those from previous work.[52] In this work, we use XRD ad EDS along with analysis of the electrochemical performance to qualify the composition of the Prussian Blue analogues. XRD analysis (Fig S3) shows that the NaPB is rhombohedral in structure while KPB has a monoclinic crystal structure. Both atomic arrangements are a result of the higher Na and K content, respectively, as the higher alkali ion concentrations force the lattices to shift into lower symmetry structures. This shift is consistent with that observed for NaPBs[35, 37, 38] and KPBs[52] intentionally synthesized with high sodium and potassium content for battery cathodes. SEM EDS spectra and mapping (Fig S4-7) supports electrochemical observations to suggest that the composition of the Prussian Blue analogues are Na_xPB, $x > 1.9$ and K_xPB, $x < 1.7$."

A rate study was conducted for both NaPB and KPB half cells to probe the rate-capability of the individual working electrodes (Fig. 2 a, b, e). Both NaPB and KPB were tested at C rates spanning between 1 C to ~ 60 C, which yields charging times of ~1 minute (Fig. 2e). At rates near 1 C, both NaPB and KPB exhibit storage capacity of ~110 mAh/g, while at the highest rate (58.8 C) the NaPB maintains a capacity of ~38 mAh/g and the KPB exhibits ~31 mAh/g.

As half-cell performance confirms material stability of both the NaPB and KPB and reflects the stability of the electrode material over a certain set of testing conditions, full-cell batteries require a combination of electrode/electrolyte compatibility, high Coulombic efficiency, and minimal first cycle loss such that the alkali metal shuttling between the electrodes actively participate in the intercalation reactions. In this spirit, we tested Na and K full-cells, GR|$NaPF_6$

in DEGDME|NaPB and GR|KPF_6 in DEGDME|KPB. A rate study with the full-cells was conducted to examine the electrochemical performance at high rates and corresponding capacities. Galvanostatic charge-discharge curves (Fig. 3 a, b) represent the measured cell capacity with respect to the cathode (NaPB) and both electrodes (FullCell). The latter case represents the actual full-cell capacity of the device, even though the former is commonly reported in the literature. Notably, for the Prussian blue system[37, 43, 44] as with other commercially viable battery systems such as the lithium nickel manganese oxide and graphite cells,[53] there are distinct differences between half cell and full cell testing. In the case of full cells, the alkali metal abundance is limited to that which originates in the cathode material. As such, SEI formation will consume some amount of this metal and slightly lower the full cell capacity from that measured in half cell tests. Further, the SEI formed on the electrodes in a full cell device can also be different, leading to diverse SEI layers that can modify kinetics and diffusion in the full cell.[54]

All batteries were cycled between rates of 1.2 C to 17.7 C, with the applied current calculated with respect to the cathode material. The energy density (E) was assessed based on the relation:

$$E = \mathrm{I}/M \int_0^{\mathrm{t}} V(t)dt$$

where M is the total combined electrode mass, V(t) is the voltage during galvanostatic testing, and I is the (constant) current used for the galvanostatic measurement. The energy density is shown in Fig. 3c at different charging/discharging rates. From this data, we observe the energy density of the Na and K batteries to be ~ 110 Wh/kg at rates of 1.2 C to energy density of ~ 75 Wh/kg for NaPB|GR and ~30 Wh/kg for KPB|GR at the fastest charging rate of 17.7 C. Cycling coulombic efficiencies and first cycle decay can be found in Fig. S11 and S12, respectively.

Although there are many factors that contribute to the rate capability of the system,[55, 56] we attribute the lower reversible capacity, and consequently lower energy density, of the KPB|GR battery at high rates to larger charge transfer resistance (Fig. S14). Especially at high rates, there can be additional electrolyte consumption as a result of joule heating due to oxygen reactions that occur at the end of fully charging the device,[57] even though our full cell devices at lower rates of 1.2 C show excellent stability and high Coulombic efficiency (Figure S11). This demonstrates the promise of this open framework/co-intercalation architecture design for full cell batteries.

To characterize the durability of these fast-charging batteries, each of these devices were subjected to extended high rates of 2 A/g, or ~ 11 C (Fig. 4a). The NaPB|GR full-cell maintained a capacity retention approaching ~ 80% over 2000 cycles and the KPB|GR full-cell retained nearly 60% capacity. This emphasizes cycling performance, especially for the NaPB|GR, promising for technological applications where augmented power capability can be achieved with comparable cycling duration to existing battery systems. It should also be noted that safety is often highlighted as a challenge in high power operation of Li batteries, with one reason for this being the non-uniform deposition of Li that occurs under high currents. In such systems, dendrite formation originates from the anode as the local host insertion lattice achieves full capacity and Li metal plating occurs on the anode surface. Whereas this is problematic for Li cells since Li metal plating in liquid electrolytes is unstable, leading to dendrite formation, the less negative electrochemical potential of Na/Na+ compared to Li/Li+ leads to dendrite-free and stable plating processes that occur within the electrochemical window of glyme electrolytes.[33, 58] This implies that, at least for fast-charging Na batteries, such non-uniform deposition will not lead to adverse safety concerns that remain problematic for fast charging Li batteries, even

though this could be a concern for the fast charging K batteries since K metal plating is similarly unstable.[59, 60]

To understand how our results compare to other high power approaches discussed in the literature, we have plotted our results compared to others who have reported full-cell battery performance (Fig. 4b). Recent reports by Jiang et al. (blue squares, Fig. 4b) and Wang et al. (blue circles, Fig. 4b) have demonstrated Prussian blue and Prussian white cells with energy densities of 150 Wh/kg and 206 Wh/kg, respectively. However, in both cases the cell performance remains limited to rates less than 0.5 A/g. Alternatively, Le Comte et al. (Orange hexagons, Fig. 4b) reported long term cycling for over 60,000 cycles at 5 C but with lower energy densities of ~11 Wh/kg and power densities on par with those reported in this work. Other works reporting NIC and KIC performance generally yield competitive or lower performance compared to our study, as is observed in Figure 4b. When comparing the devices from this study with other electrochemical energy storage devices (Figure 4c), it is evident that the energy density is on par with and the power density is higher than that of battery technologies. Even when considering the mass contributions from packaging, the power and energy densities are still improved over current battery technologies. In our study, we demonstrate the feasibility for a battery system to enable both high rate performance and moderate energy densities with the possibility to further tune and optimize both the open framework cathode structure, as well as the electrode-electrolyte interface that enables co-intercalation to engineer the performance characteristics in the framework of this general fast-charging battery design scheme.

Conclusion

In summary, here we have demonstrated how a co-intercalation natural graphite anode and an open framework Prussian blue cathode can enable high-power batteries with moderate

energy density >100 Wh/kg and power density > 1000 W/kg. Using a co-intercalation anode, 1) eliminates the rate-limiting step of alkali ion de-solvation at the electrode-electrolyte interface, allowing for high rate capability and 2) allows for alternative ion intercalation into graphitic carbon. Prussian blue as a cathode material offers a rigid, open framework with large interstitial sites for ease of rapid ion extraction and insertion, supporting both Na and K chemistries.

The synergy of these electrode materials holds great promise for high-power batteries for electric vehicles and efficient storage of renewable energy. Further investigation into refining the cathode material allows for tunability to access a broad range of power and energy densities currently outside the scope of traditional supercapacitor and battery systems. This study lays the groundwork for engineering an electrode/electrolyte system for fast-charging, energy-dense batteries that overcome the limitations of supercapacitors and enable performance as a battery at high currents or under fast-charging conditions.

Conflict of Interest

There are no conflicts to declare.

Supporting Information

Supporting information is available and contains (1) experimental images of the PB synthesis, (2) scanning electron imaging, and (3) galvanostatic rate-study of the natural graphite half cells.

Acknowledgments

The authors acknowledge Mengya Li, Keith Share, and Kody Wolfe for helpful discussions, and the laboratory facilities of Rizia Bardhan. This work was supported in part by NSF grant CMMI 1400424, and A.P.C. was supported by NSF graduate fellowships under grant 1445197.

References

1. H. Li, Y. Zhu, S. Dong, L. Shen, Z. Chen, X. Zhang and G. Yu, *Chem. Mater.*, 2016, **28**, 5753-5760.
2. J. Lang, X. Zhang, B. Liu, R. Wang, J. Chen and X. Yan, *J. Energy Chem.*, 2018, **27**, 43-56.
3. B. Kang and G. Ceder, *Nature*, 2009, **458**, 190-193.
4. Y. Ding, B. Yang, J. Chen, L. Zhang, J. Li, Y. Li and X. Yan, *Science China Mater.*, 2017, DOI: 10.1007/s40843-017-9141-7.
5. J. Feng, N. A. Chernova, F. Omenya, L. Tong, A. C. Rastogi and M. Stanley Whittingham, *J. Solid State Electrochem.*, 2017, DOI: 10.1007/s10008-017-3847-1, 1-16.
6. A. Le Comte, Y. Reynier, C. Vincens, C. Leys and P. Azaïs, *J. Power Sources*, 2017, **363**, 34-43.
7. L. Kouchachvili, W. Yaïci and E. Entchev, *J. Power Sources*, 2018, **374**, 237-248.
8. W. Cao, Y. Li, B. Fitch, J. Shih, T. Doung and J. Zheng, *J. Power Sources*, 2014, **268**, 841-847.
9. J. Boltersdorf, S. A. Delp, J. Yan, B. Cao, J. P. Zheng, T. R. Jow and J. A. Read, *J. Power Sources*, 2018, **373**, 20-30.
10. F. Béguin, V. Presser, A. Balducci and E. Frackowiak, *Adv. Mater.*, 2014, **26**, 2219-2251.
11. L. L. Zhang and X. S. Zhao, *Chem. Soc. Rev.*, 2009, **38**, 2520-2531.

12. X. Sun, X. Zhang, H. Zhang, D. Zhang and Y. Ma, *J. Solid State Electrochem*, 2012, **16**, 2597-2603.

13. M. D. Stoller and R. S. Ruoff, *Energy Environ Sci*, 2010, **3**, 1294-1301.

14. V. Ruiz, C. Blanco, M. Granda, R. Menéndez and R. Santamaría, *J. Applied Electrochem*, 2007, **37**, 717-721.

15. E. Raymundo-Pinero, K. Kierzek, J. Machnikowski and F. Beguin, *Carbon*, 2006, **44**, 2498-2507.

16. Q. Gao, L. Demarconnay, E. Raymundo-Pinero and F. Beguin, *Energy Environ Sci*, 2012, **5**, 9611-9617.

17. E. G. Calvo, F. Lufrano, P. Staiti, A. Brigandì, A. Arenillas and J. A. Menéndez, *J. Power Sources*, 2013, **241**, 776-782.

18. N. Blomquist, T. Wells, B. Andres, J. Bäckström, S. Forsberg and H. Olin, *Sci. Rep.*, 2017, **7**, 39836.

19. J. Y. Hwang, M. F. El-Kady, M. Li, C.-W. Lin, M. Kowal, X. Han and R. B. Kaner, *Nano Today*, 2017, **15**, 15-25.

20. J. C. Pramudita, D. Sehrawat, D. Goonetilleke and N. Sharma, *Adv. Energy Mater.*, DOI: 10.1002/aenm.201602911, 1602911.

21. P. Lu, Y. Sun, H. Xiang, X. Liang and Y. Yu, *Adv. Energy Mater.*, DOI: 10.1002/aenm.201702434, 1702434

22. Z. Zhu, F. Cheng, Z. Hu, Z. Niu and J. Chen, *J. Power Sources*, 2015, **293**, 626-634.

23. B. Jache, J. O. Binder, T. Abe and P. Adelhelm, *Phys. Chem. Chem. Phys.*, 2016, **18**, 14299-14316.

24. P. Han, X. Han, J. Yao, L. Zhang, X. Cao, C. Huang and G. Cui, *J. Power Sources*, 2015, **297**, 457-463.

25. T. Kajita and T. Itoh, *Phys. Chem. Chem. Phys.*, 2018, DOI: 10.1039/C7CP06998G, 2188-2195.

26. H. Kim, J. Hong, G. Yoon, H. Kim, K.-Y. Park, M.-S. Park, W.-S. Yoon and K. Kang, *Energy Environ. Sci.*, 2015, **8**, 2963-2969.

27. H. Kim, G. Yoon, K. Lim and K. Kang, *ChemComm*, 2016, **52**, 12618-12621.

28. H. Kim, K. Lim, G. Yoon, J.-H. Park, K. Ku, H.-D. Lim, Y.-E. Sung and K. Kang, *Adv. Energy Mater.*, 2017, **7**, 1700418.

29. L. Wang, J. Zou, S. Chen, G. Zhou, J. Bai, P. Gao, Y. Wang, X. Yu, J. Li, Y.-S. Hu and H. Li, *Energy Stor. Mater.*, 2018, **12**, 216-222.

30. M. Hu, H. Zhou, X. Gan, L. Yang, Z.-H. Huang, D.-W. Wang, F. Kang and R. Lv, *J. Mater. Chem. A*, 2018, **6**, 1582-1589.

31. H. Moon, R. Tatara, T. Mandai, K. Ueno, K. Yoshida, N. Tachikawa, T. Yasuda, K. Dokko and M. Watanabe, *J. Phys. Chem. C*, 2014, **118**, 20246-20256.

32. J. Maibach, F. Jeschull, D. Brandell, K. Edström and M. Valvo, *ACS Appl. Mater. Interfaces*, 2017, **9**, 12373-12381.

33. A. P. Cohn, K. Share, R. Carter, L. Oakes and C. L. Pint, *Nano Lett.*, 2016, **16**, 543-548.

34. A. P. Cohn, N. Muralidharan, R. Carter, K. Share, L. Oakes and C. L. Pint, *J. Mater. Chem. A*, 2016, **4**, 14954-14959.

35. Y. Tang, W. Zhang, L. Xue, X. Ding, T. Wang, X. Liu, J. Liu, X. Li and Y. Huang, *J. Mater. Chem. A*, 2016, **4**, 6036-6041.

36. Y. Liu, Y. Qiao, W. Zhang, Z. Li, X. Ji, L. Miao, L. Yuan, X. Hu and Y. Huang, *Nano Energy*, 2015, **12**, 386-393.

37. L. Wang, J. Song, R. Qiao, L. A. Wray, M. A. Hossain, Y.-D. Chuang, W. Yang, Y. Lu, D. Evans, J.-J. Lee, S. Vail, X. Zhao, M. Nishijima, S. Kakimoto and J. B. Goodenough, *J. Am. Chem. Soc.*, 2015, **137**, 2548-2554.

38. Y. You, X.-L. Wu, Y.-X. Yin and Y.-G. Guo, *Energy Environ. Sci.*, 2014, **7**, 1643-1647.

39. M. J. Piernas-Muñoz, E. Castillo-Martínez, O. Bondarchuk, M. Armand and T. Rojo, *J. Power Sources*, 2016, **324**, 766-773.

40. X. Qiu, Y. Liu, L. Wang and L.-Z. Fan, *Appl. Surf. Sci.*, 2018, **434**, 1285-1292.

41. H. Kim, J. C. Kim, M. Bianchini, D.-H. Seo, J. Rodriguez-Garcia and G. Ceder, *Adv. Energy Mater.*, DOI: 10.1002/aenm.201702384, 1702384.

42. Y. You, X. Yu, Y. Yin, K.-W. Nam and Y.-G. Guo, *Nano Res.*, 2015, **8**, 117-128.

43. Y. Jiang, S. Yu, B. Wang, Y. Li, W. Sun, Y. Lu, M. Yan, B. Song and S. Dou, *Adv. Funct. Mater.*, 2016, **26**, 5315-5321.

44. C. Zhang, Y. Xu, M. Zhou, L. Liang, H. Dong, M. Wu, Y. Yang and Y. Lei, *Adv. Funct. Mater.*, 2017, **27**, 1604307.

45. X. Wu, D. P. Leonard and X. Ji, *Chem. Mater.*, 2017, **29**, 5031-5042.

46. Y. Lu, L. Wang, J. Cheng and J. B. Goodenough, *ChemComm*, 2012, **48**, 6544-6546.

47. X. Bie, K. Kubota, T. Hosaka, K. Chihara and S. Komaba, *J. Power Sources*, 2018, **378**, 322-330.

48. C. D. Wessells, S. V. Peddada, R. A. Huggins and Y. Cui, *Nano Lett.*, 2011, **11**, 5421-5425.

49. J. Qian, C. Wu, Y. Cao, Z. Ma, Y. Huang, X. Ai and H. Yang, *Adv. Energy Mater.*, DOI: 10.1002/aenm.201702619, 1702619.

50. C. Li, R. Zang, P. Li, Z. Man, S. Wang, X. Li, Y. Wu, S. Liu and G. Wang, *Chem. Asian J.*, 2018, **13**, 342-349.

51. J. L. Xueying Yang, Xinkun Song, Yingzhao He, Xiaoxiao Du, Yongjin Zou, Haitao Zhang, *Int. J. Nanoparticles Nanotech*, 2017, **3**, 011.

52. G. He and L. F. Nazar, *ACS Energy Lett.*, 2017, **2**, 1122-1127.

53. J. Wang, J. Purewal, P. Liu, J. Hicks-Garner, S. Soukazian, E. Sherman, A. Sorenson, L. Vu, H. Tataria and M. W. Verbrugge, *J. Power Sources*, 2014, **269**, 937-948.

54. P. L. Taberna, S. Mitra, P. Poizot, P. Simon and J. M. Tarascon, *Nature Materials*, 2006, **5**, 567.

55. J. W. McCargar and V. D. Neff, *The Journal of Physical Chemistry*, 1988, **92**, 3598-3604.

56. C. D. Wessells, S. V. Peddada, M. T. McDowell, R. A. Huggins and Y. Cui, *J. Electrochem. Soc.*, 2011, **159**, A98-A103.

57. W. B. Gu and C. Y. Wang, *J. Electrochem. Soc.*, 2000, **147**, 2910-2922.

58. A. P. Cohn, N. Muralidharan, R. Carter, K. Share and C. L. Pint, *Nano Lett.*, 2017, **17**, 1296-1301.

59. J. Cannarella and C. B. Arnold, *J. Electrochem. Soc.*, 2015, **162**, A1365-A1373.

60. X. M. Liu and C. B. Arnold, *J. Electrochem. Soc.*, 2016, **163**, A2501-A2507.

Figures

Figure 1

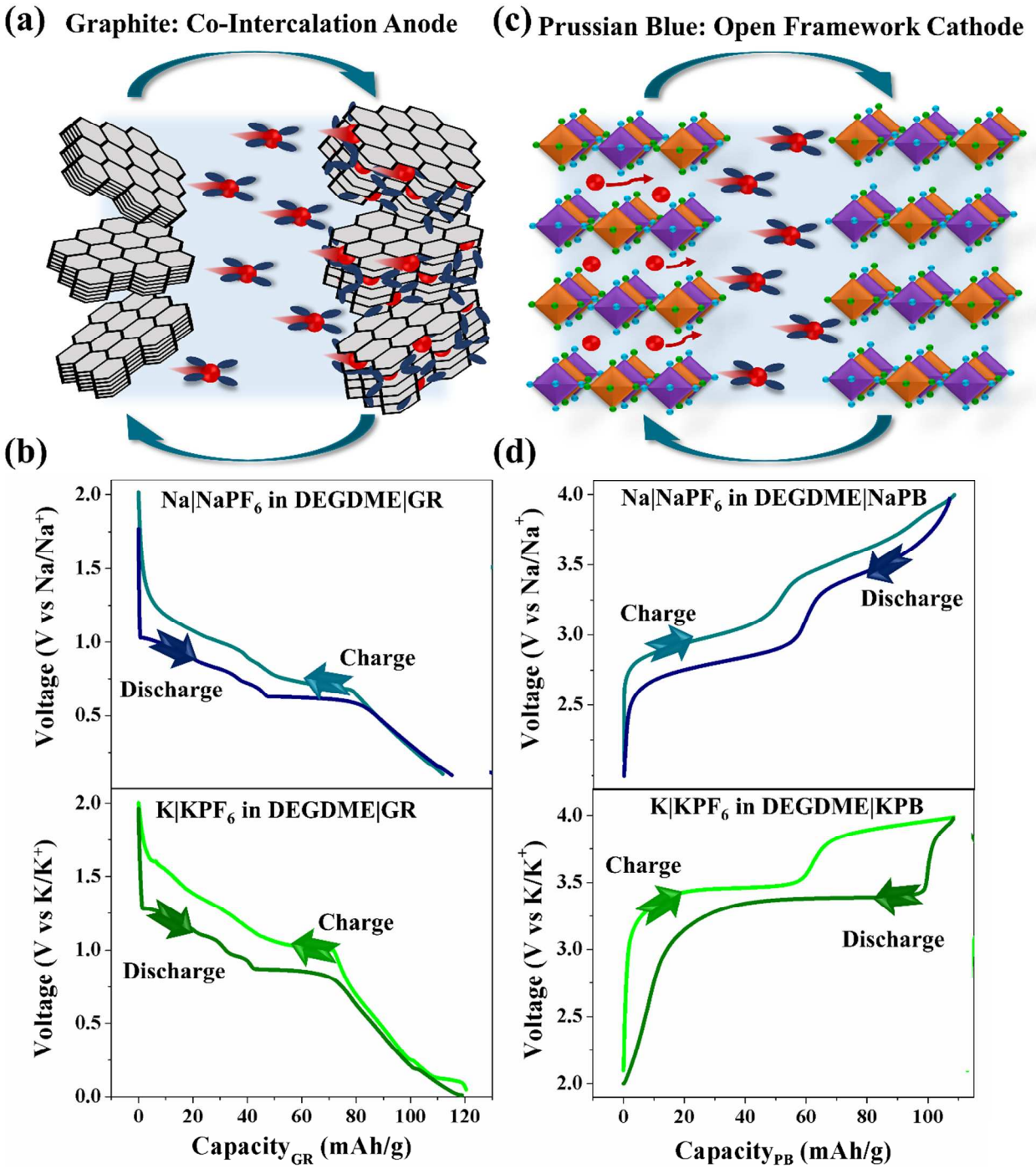

Figure 1: Diglyme electrolyte solvent is compatible with both anode and cathode chemistries, confirmed by galvanostatic charge-discharge curves of both Na and K chemistries of (b) natural graphite and (d) Prussian blue.

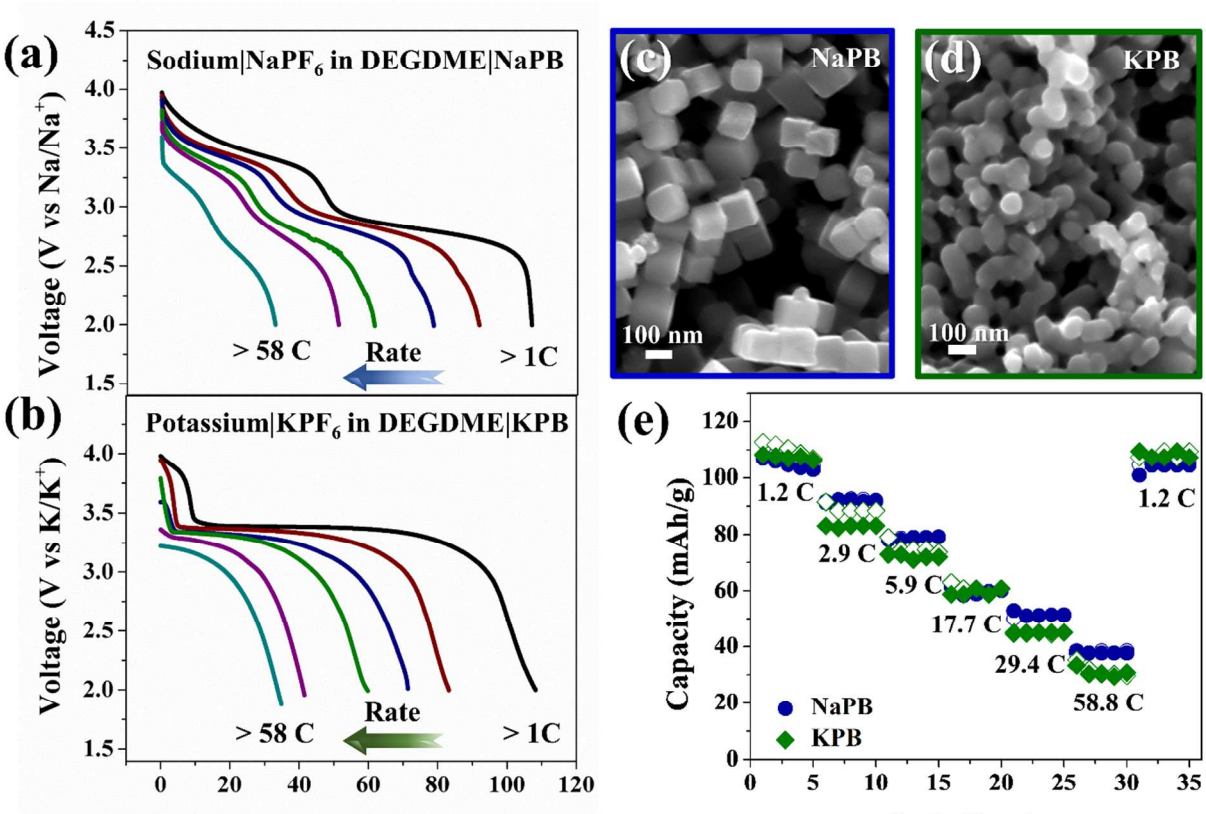

Figure 2: Prussian blue cathode supports both Na and K chemistries for high rate capability demonstrated by the synthesized (c) NaPB and (d) KPB nanoparticles and their corresponding electrochemical performance (a, b, e).

Figure 3

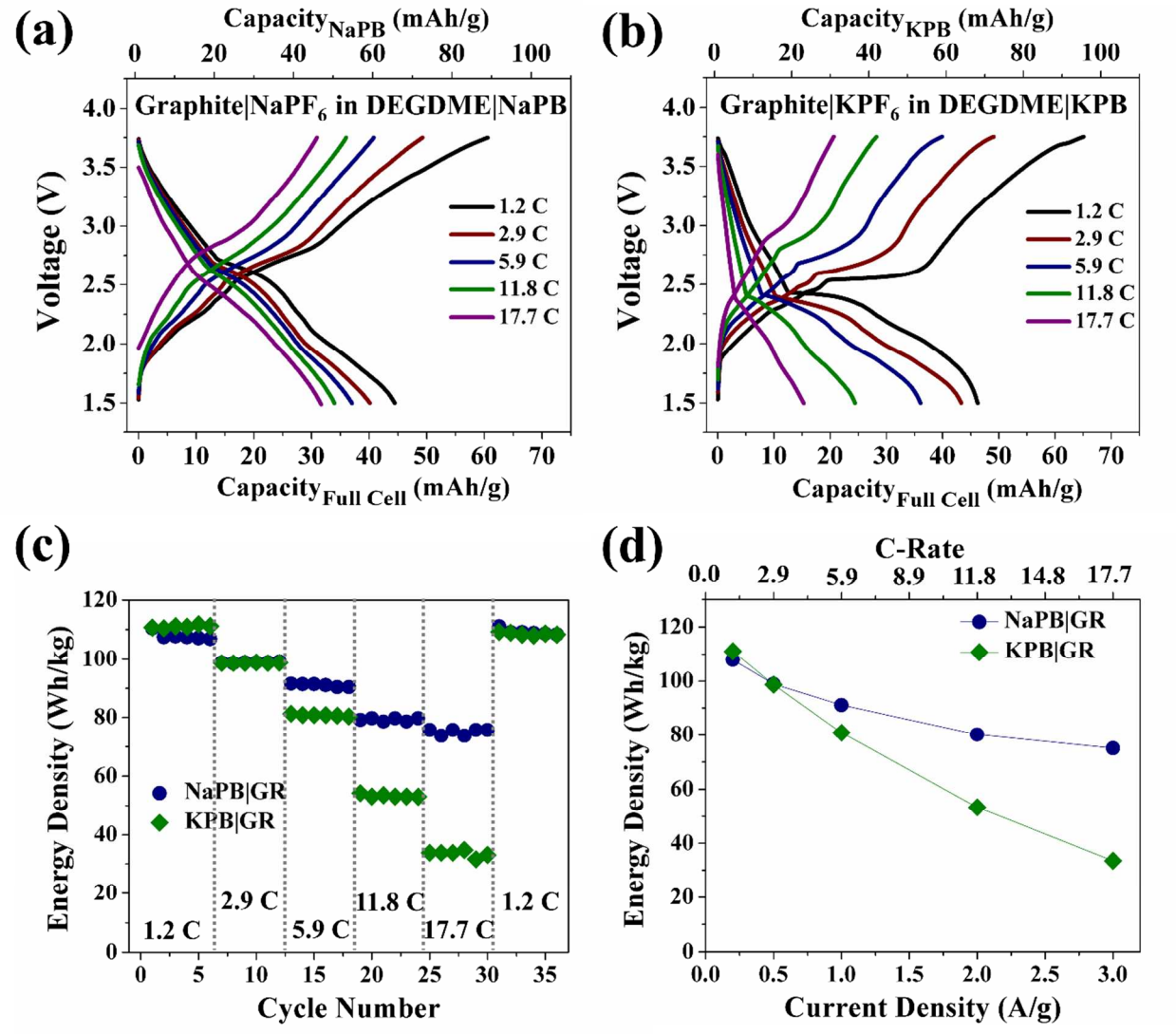

Figure 3: Electrochemical performance of rate study of GR|PB full cell, galvanostatic charge-discharge curves of 1st cycle of each rate for (a) Na and (b) K chemistries, (c) corresponding plot of energy density at cycle, and (d) average energy density at each rate.

Figure 4

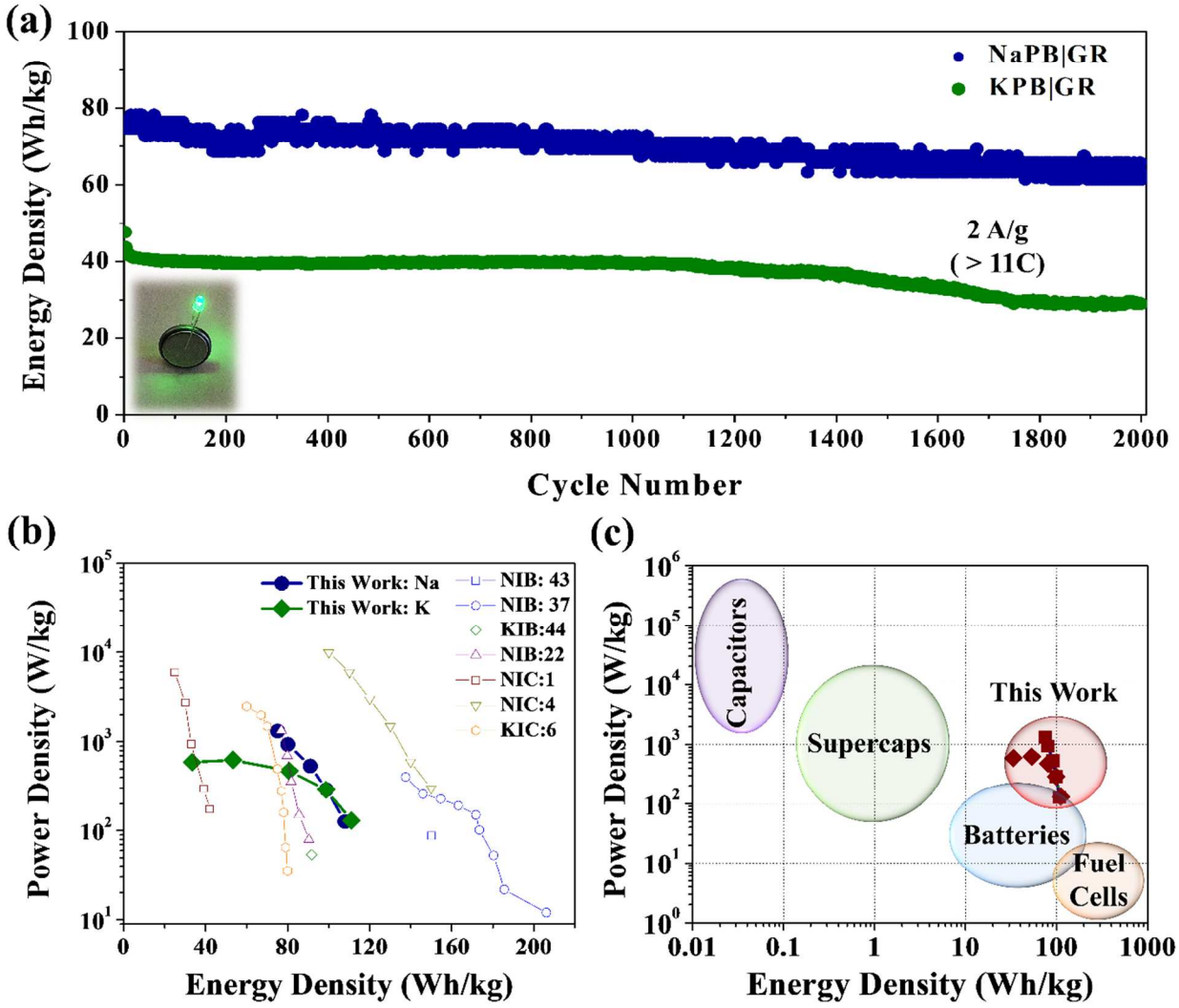

Figure 4: Full cell high rate capability for extended cycling at (a) 2 A/g for 2000 cycles with an inset of a lit green light LED, (b) this work compared to literature, and (c) this work compared with other electrochemical energy storage devices.

TOC

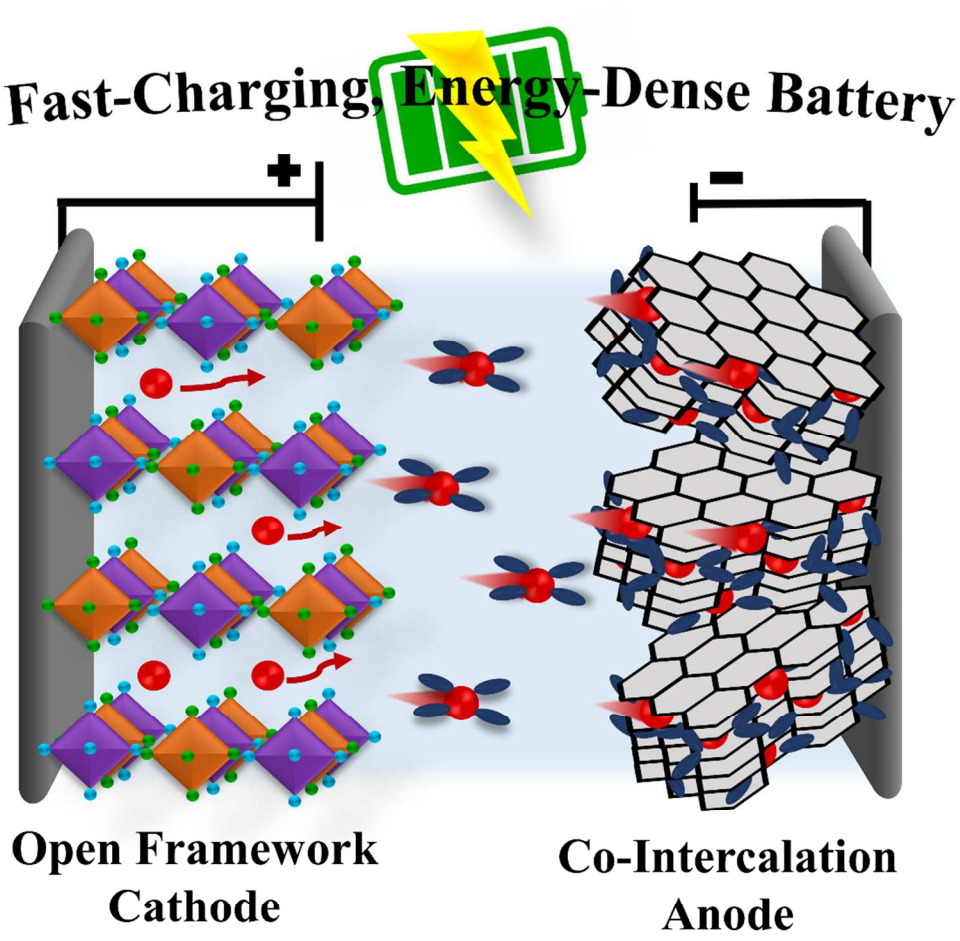

Theme: A fast-charging full-cell battery design is demonstrated that builds upon ultrafast metal ion co-intercalation at the anode and fast ion diffusion through an open framework structure at the cathode to enable high power cycling with moderate energy densities approaching 100 Wh/kg.